International Journal of Thermophysics, Vol. 3, No. 3, 1982

Transient Interferometric Technique for Measuring Thermal Expansion at High Temperatures: Thermal Expansion of Tantalum in the Range 1500–3200 K

A. P. Miiller[1] and A. Cezairliyan[1]

Received April 23, 1982

The design and operational characteristics of an interferometric technique for measuring thermal expansion of metals between room temperature and temperatures in the range 1500 K to their melting points are described. The basic method involves rapidly heating the specimen from room temperature to temperatures above 1500 K in less than 1 s by the passage of an electrical current pulse through it, and simultaneously measuring the specimen expansion by the shift in the fringe pattern produced by a Michelson-type polarized beam interferometer and the specimen temperature by means of a high-speed photoelectric pyrometer. Measurements of linear thermal expansion of tantalum in the temperature range 1500–3200 K are also described. The results are expressed by the relation:

$$(l - l_0)/l_0 = 5.141 \times 10^{-4} + 1.445 \times 10^{-6}T + 4.160 \times 10^{-9}T^2$$

$$- 1.309 \times 10^{-12}T^3 + 1.901 \times 10^{-16}T^4$$

where T is in K and l_0 is the specimen length at 20°C. The maximum error in the reported values of thermal expansion is estimated to be about 1% at 2000 K and not more than 2% at 3000 K.

KEY WORDS: high temperature; interferometry; pulse heating; tantalum; thermal expansion.

1. INTRODUCTION

There has been an increasing need in recent years for thermal expansion data on refractory materials at temperatures above the limit of accurate steady-state experiments. Fizeau interferometric methods yield expansion

[1] Thermophysics Division, National Bureau of Standards, Washington, D.C. 20234, U.S.A.

0195-928X/82/0900-0259$03.00/0

data with high precision but are limited to temperatures below about 1100 K by practical considerations. At higher temperatures, expansion measurements are usually performed by other steady-state techniques such as push-rod dilatometry, x-ray diffractometry, or the twin-telemicroscope method. In these techniques, the specimen is exposed to elevated temperatures for extended periods of time (minutes to hours), thereby creating problems associated with the increased heat transfer, loss of mechanical strength, evaporation, chemical reactions, etc., which become particularly severe at temperatures above 2000 K. One approach to minimize the effect of these problems is to use a rapid measurement technique in which the entire experiment is performed in a very short period of time (less than 1 s).

During the last decade, considerable progress has been made in the development of high-speed methods in which the specimen is resistively heated by means of a subsecond-duration pulse of electrical current. Such transient techniques have been used for accurate measurements of selected thermophysical properties including heat capacity, electrical resistivity, and thermal radiative properties of a number of electrically conducting refractory materials at temperatures up to their melting points [1]. However, high-speed methods have not, as yet, been used for accurate measurements of the thermal expansion of solids because of the lack of high-precision techniques for measuring rapid changes in the specimen "length." Prior to the present work, a few investigators [2, 3] have used photographic techniques for high-speed measurements of thermal expansion. Some preliminary work involving a photometric technique [4] has also been reported.

The application of interferometry to high-speed measurements of thermal expansion was first reported by Ruffino et al. [5], in 1974. Their method was based on following the motion of two fiducial holes in the specimen during its rapid heating by means of servo-mechanically driven image followers and measuring the varying distance between the image followers with a Michelson interferometer. Unfortunately, difficulties arising from uncertainties in the time response of the servo-mechanisms have tended to limit the usefulness of the method for accurate subsecond experiments.

A few years ago, we began the development of an accurate high-speed interferometric technique for the purpose of measuring thermal expansion of electrically conducting solids at high temperatures, primarily in the range 1500 K to the melting point of the specimen. This involved adapting a Michelson-type interferometer to the existing pulse heating system [6, 7] at the National Bureau of Standards (NBS). The feasibility of the method was demonstrated by preliminary measurements [8] on the thermal expansion of tantalum over a limited temperature range.

The basic method involves rapidly heating the specimen from room temperature to the maximum temperature of interest in less than 1 s by the passage of an electrical current pulse through it, and simultaneously measuring the specimen temperature by means of a high-speed photoelectric pyrometer [9] and the shift in the fringe pattern produced by the interferometer. The polarized beam from a He-Ne laser in the interferometer is split into two component beams, one which undergoes successive reflections from optical flats on opposite sides of the specimen, and one which serves as the reference beam. The linear thermal expansion of the specimen is then determined from the cumulative fringe shift corresponding to a given specimen temperature.

In this paper, we present a detailed description of the design and construction of our thermal expansion measurement system, including modifications and improvements that have been subsequently made to the interferometric system developed during the earlier feasibility study. The results from a series of experiments on the thermal expansion of tantalum at temperatures between 1500 and 3200 K are also given. The purpose of the present measurements on tantalum is twofold: (1) to assess the operational characteristics of the interferometric system over a large temperature range, particularly at temperatures approaching the melting point of the specimen, and (2) to obtain accurate expansion values for tantalum at temperatures where considerable disagreement exists among data reported in the literature.

2. MEASUREMENT SYSTEM

The thermal expansion measurement system consists of: (1) a pulse-heating system which includes an electric power-pulsing circuit, a high-speed pyrometer, and associated measurement and control circuits; and (2) an interferometric system which includes a two-beam interferometer and a phase-quadrature detector. A functional diagram of the measurement system and a photograph of part of the system are presented in Figs. 1 and 2, respectively.

2.1. Pulse-Heating System

Details regarding the construction and operation of the pulse-heating system at NBS are given in earlier publications [6, 7]. In this paper, we briefly describe only those features pertinent to the measurement of thermal expansion.

The power-pulsing circuit consists of the specimen in series with a battery bank, an adjustable resistance (water-cooled Inconel tube), and a

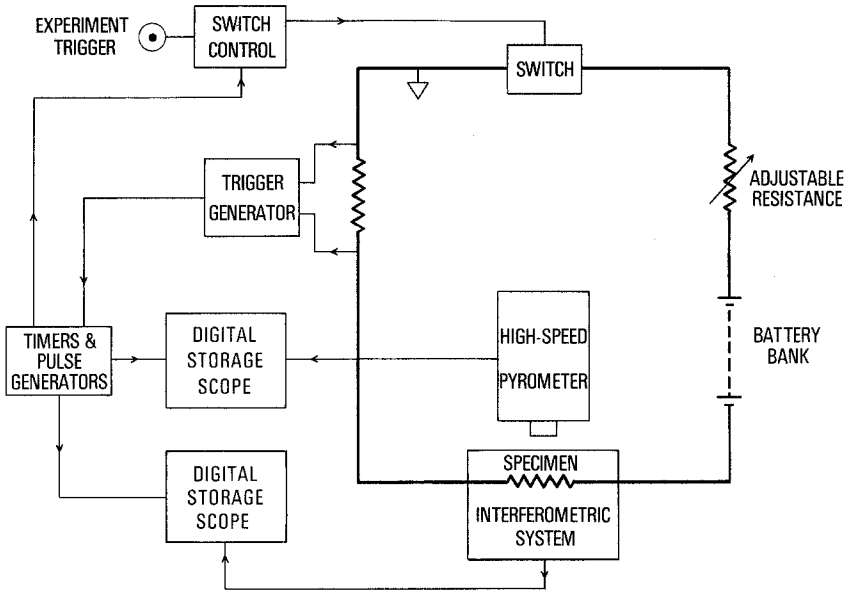

Fig. 1. Functional diagram of the system for high-speed interferometric measurement of thermal expansion.

fast-acting switch. Adjustments, prior to pulse heating, of the battery bank voltage (up to 26 V) and the length, hence resistance (0–30 mΩ), of the Inconel tube in the circuit enable control of the specimen heating rate. The timing of various events, such as closing and opening of the switch and triggering of electronic equipment, is achieved by means of electronic logic circuits and a series of time delay units.

The temperature of the specimen is measured with a high-speed photoelectric pyrometer [9], which permits 1200 evaluations of specimen temperature per second. A rapidly rotating chopper disk in the pyrometer alternately passes precisely timed samples of radiance from the specimen and from a tungsten-filament reference lamp through an interference filter to a photomultiplier. During each exposure, the output of the photomultiplier is integrated and then recorded by a digital storage oscilloscope (see Section 2.5). The effective wavelength of the pyrometer's interference filter is 653 nm, with a bandwidth of 10 nm. The circular area viewed by the pyrometer is 0.2 mm in diameter.

2.2. Specimen

The specimen is fabricated into the form of a precision-machined tube with parallel optical flats on opposite sides for the interferometric measure-

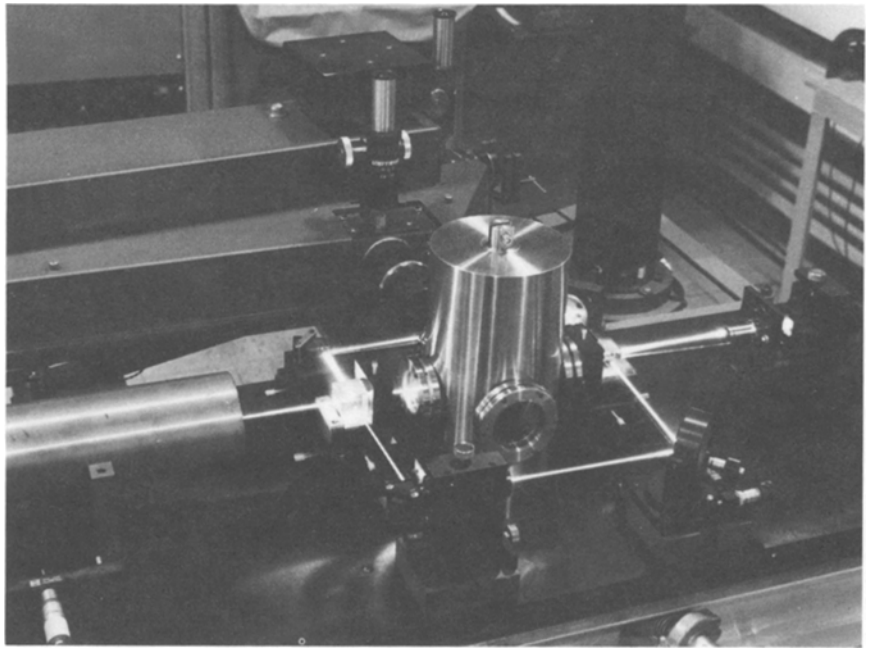

Fig. 2. Photograph of the polarized-beam interferometer, high-speed pyrometer, and specimen chamber.

ments. A cross-section through the middle of the specimen is illustrated in Fig. 3. The nominal dimensions of the tube are: length, 76 mm; inside diameter, 5.3 mm; outside diameter, 6.8 mm; distance between parallel optical flats, 6.1 mm. The latter dimension is the specimen "length" referred to in the description of the interferometer (next section). A small rectangular sighting hole (0.5×1 mm) is fabricated through the wall at the middle of each tube, thereby approximating blackbody conditions for optical temperature measurements. The sighting hole is fabricated 0.8 mm off center from the tube axis to improve the blackbody quality. In order to compensate for the cross-sectional nonuniformity created by the hole, a portion of the specimen is removed by grinding a flat along the length of the tube, excluding the 1 mm length of the hole.

The specimen is mounted vertically, as shown in Fig. 4, in a test chamber designed for experiments either in a vacuum or in a controlled atmosphere. Water-cooled end-clamps connect the specimen to electrodes: a stationary upper electrode and a lower electrode, which is connected through a linear guide to a flexible connection. This arrangement allows for thermal expansion of the specimen along its length in the downward

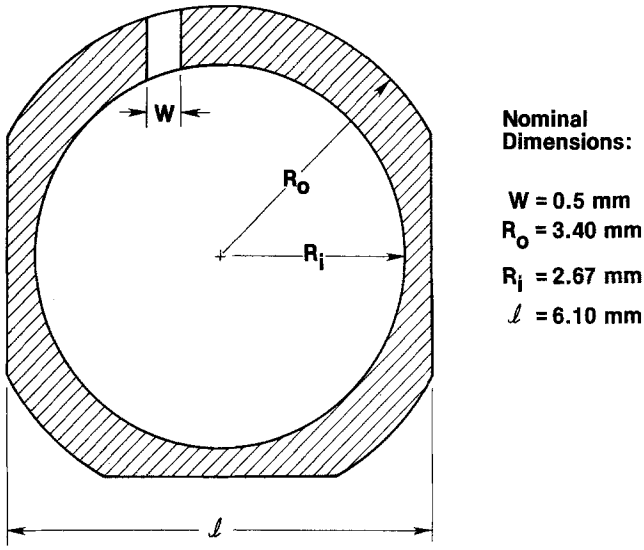

Fig. 3. Specimen cross-section in the plane of the interferometer. The distance l between parallel optical flats is the specimen "length."

direction without significant rotational movement that might otherwise arise from the mechanical and electromagnetic forces present during rapid pulse heating. The rotational stability of the specimen during a pulse experiment is determined by reflecting the beam of an auxiliary laser from a third optical flat (directly opposite from the pyrometric sighting hole) on the specimen and measuring the displacement of the reflected beam (discussed in the Appendix). The "room" temperature of the specimen prior to each experiment is measured by thermocouples connected to the end-clamps.

2.3. Interferometer

The interferometer is a modified Michelson interferometer with the specimen acting as a double reflector in the path of one of the two light beams, as illustrated schematically in Fig. 5. The coherent light source is a plane-polarized He-Ne laser (2 mW).

A polarizing beam-splitter PB1 separates the linearly polarized beam from the laser into two component beams. The component polarized normal to the plane of the interferometer (s-polarized) is reflected around the specimen area and into the detector by PB1, the pentaprism/lens combination PP1/L3/L4, plane mirror M1, and a second polarizing beamsplitter PB2; it therefore serves as the reference beam. The other

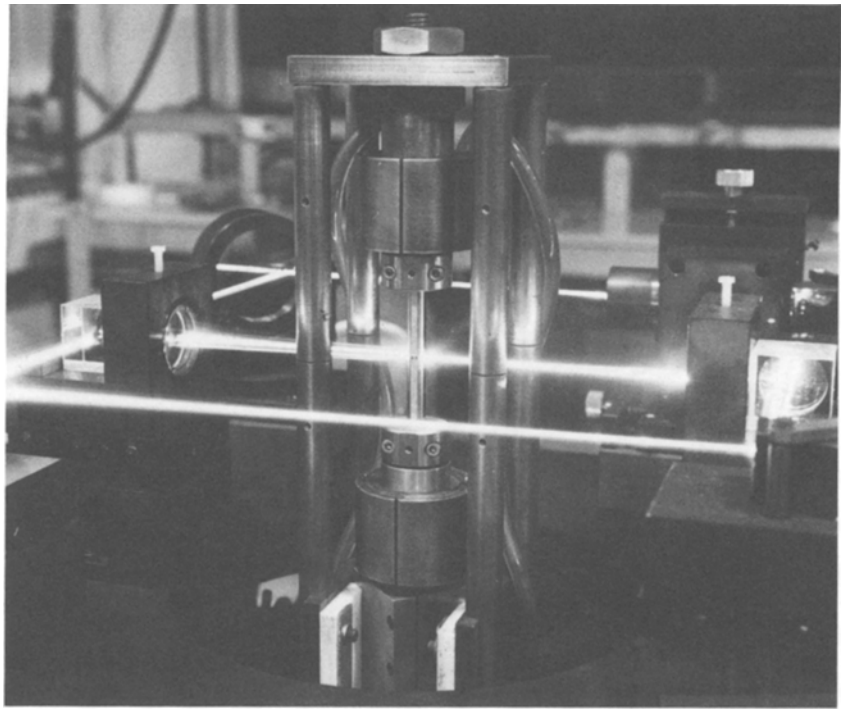

Fig. 4. Photograph of the specimen mounted vertically between a stationary upper electrode and a lower electrode which is attached to a flexible connection through a linear guide.

component beam, polarized parallel to the interferometer plane (p-polarized), is transmitted by PB1 and is directed through quarter-wave plate QP1, which has its principal axis oriented at 45° to the polarization planes. The emergent circularly polarized beam is focused by lens L1 onto the polished "front" surface of the specimen where, upon reflection at normal incidence, the sense of circular polarization is reversed. After a second pass through QP1 the beam is again linearly polarized, but now with s-polarization so that it can be reflected around the specimen by PB1, pentaprism PP2, and mirror M2. By similar consideration of the optical elements PB2, QP2, and L2, one can show that after reflection from the "back" surface of the specimen, the component beam ultimately emerges from the interferometer and enters the detector with its original polarization, that is, p-polarization.

It is important to note that the optical path length of the "specimen" beam is independent of rigid body translations by the specimen because of

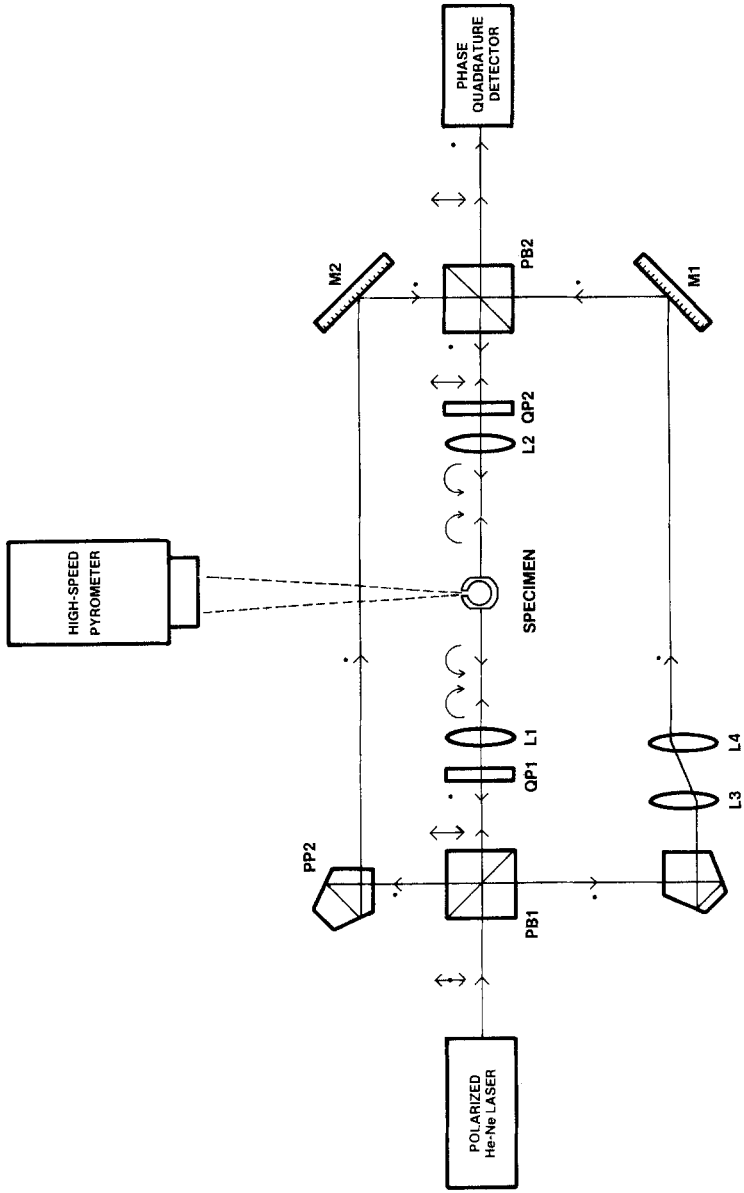

Fig. 5. Schematic diagram of the interferometer consisting of the following optical elements: polarizing beamsplitters PB1 and PB2; quarter-wave plates QP1 and QP2; lenses L1, L2, L3, and L4; pentaprisms PP1 and PP2; and plane mirrors M1 and M2. The double-headed arrows, the heavy dots, and the curved arrows refer to the polarization states of the component beams.

the successive front surface/back surface reflections. Therefore, the interferometer is inherently insensitive to translational motion of the specimen, which may be generated by the passage of a large current pulse through the specimen.

The initial step in the alignment of the interferometer involves translational adjustments of PP2 and angular adjustments of M2 to ensure that the beams incident upon opposite sides of the specimen are colinear. The reference beam (s-polarization) is then superimposed with the "specimen" beam (p-polarization) by horizontal and vertical translations of the pentaprism/lens combination PP1/L3/L4 and rotational adjustments of M1.

An important function of lenses L1 and L2 is to minimize the sensitivity of the interferometer to any rotational movements of the specimen that may occur during a pulse experiment. If the focal planes of L1 and L2 coincide with the optical flats on the specimen, the "specimen" beam will remain superimposed with the reference beam at the detector irrespective of (small) rotational movements by the specimen (see the Appendix). Of course, such rotational movement will create an apparent change in the "length" of the specimen. It is demonstrated in the Appendix that the colinear alignment of beams incident upon the specimen is very important in minimizing the effect of possible specimen rotation on the results.

The light output of the interferometer, therefore, consists of two superimposed beams, which are polarized mutually at right angles. One can readily observe interference between the two beams by placing an analyzer with its principal axis at 45° with respect to the polarization directions in the path of the emergent beams; only the component of electric field vector resolved in the 45° direction for each beam is transmitted by the analyzer. The path difference (PD) or phase difference (δ) between the beams is the same at all points in the field of view insofar as the interferometer can be adjusted to produce circular fringes of "infinite breadth." In principle, this may be accomplished by small adjustments in the separation between L3 and L4 so that the wavefront curvature of the reference beam is the same as that for the "specimen" beam. In practice, however, very small differences in wavefront curvature remain so that very broad circular fringes are seen instead. The light intensity is essentially uniform across the field of view, becoming maximum or minimum, respectively, whenever

$$PD = n\lambda \quad \text{or} \quad PD = (n + 1/2)\lambda \tag{1}$$

where λ is the wavelength and $n = 0, 1, 2, \ldots$. The contrast between the bright and dark fringes is maximized by rotating the plane of polarization of the input beam from the laser in order to compensate for unequal light

losses along the paths of the two beams. It follows from Eq. (1) that any change in path difference will yield a shift in the fringe pattern according to

$$\Delta PD = \lambda \Delta n \tag{2}$$

where Δn is the number of fringes (bright or dark) that shift through the field of view.

As the specimen is rapidly heated through a temperature interval ΔT, its "length" l changes by an amount Δl, thereby giving rise to a change in the path difference of

$$\Delta PD = 2\Delta l \tag{3}$$

Combining Eqs. (2) and (3), one can express the fractional linear expansion of the specimen as

$$(l - l_0)/l_0 = (\lambda/2l_0)\Delta n \tag{4}$$

where l_0 is the length of the specimen at some reference temperature (20°C).

The linear thermal expansion of metals between room temperature and their melting points is typically in the range 2–2.5% which, for the specimen "length" (6.1 mm) and wavelength (632.8 nm) used in our measurement technique, corresponds to a cumulative fringe shift of about 400–500 fringes. Since the fringe shift occurs in a time interval of less than 1 s, a high-speed photodetection system is required to accurately record the fringe movements.

2.4. Phase-Quadrature Detector

A number of arrangements are possible for deriving signals in phase quadrature from the light output of an interferometer so that bidirectional counting of the interference fringe movements can be carried out [10, 11]. The detector design used in our interferometric system is similar in principle to one developed by Hocken [12] at NBS. The phase-quadrature detector, shown schematically in Fig. 6, consists of a beam expander, an interference filter, a quarter-wave plate, a four-quadrant analyzer, and a four-element silicon photodiode, each element converting the light passed by one analyzer quadrant into an electrical signal.

Thermal radiation from the specimen during pulse heating is largely removed from the component beams entering the detector by means of an interference filter with a narrow passband (1 nm) centered at the laser wavelength (632.8 nm). The effect of residual background radiation passed

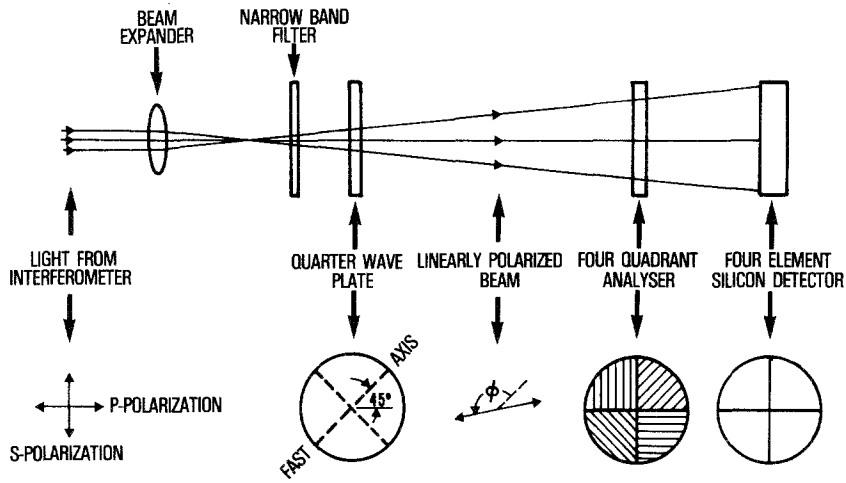

Fig. 6. Schematic diagram of the phase quadrature detector.

by the filter is eliminated by differential amplification of the electrical signals from diagonally opposite elements of the photodiode (see below).

The key optical components of the detector are the quarter-wave plate with its optic or fast axis at 45° to the (linear) polarization directions and the four-quadrant analyzer with principal axes rotated by increments of 45° in successive quadrants as shown in Fig. 6. The quarter-wave plate converts the linear polarizations of the reference and "specimen" beams from the interferometer into left- and right-handed circular polarizations, respectively. If the intensities of the two beams from the interferometer are adjusted to be equal, the two circularly polarized beams combine into a single linearly polarized beam whose polarization orientation ϕ is linearly dependent on the phase difference δ between the beams entering the detector. It can be shown that if ϕ is measured counter-clockwise (c.c.w.) from the direction of the fast axis of the quarter-wave plate, then

$$\phi = \delta/2 \tag{5}$$

Therefore, as δ changes by $+2\pi$ or -2π rad, the polarization plane of the light reaching the analyzer will rotate through $+\pi$ or $-\pi$ rad, and so the light transmission through the four quadrants will undergo one cycle around the quadrants in a c.c.w. or clockwise (c.w.) direction. In terms of terminology used in the previous section, this corresponds to a shift of one fringe into or out of the field of view.

In general, the intensities of the component beams leaving the interferometer are not exactly equal. In other words, the amplitudes of electric field

vibrations corresponding to the reference (s-polarized) and "specimen" (p-polarized) beams, E_s and E_p respectively, are somewhat different. In this case the linearly polarized component beams are converted by the quarter-wave plate into left and right circularly polarized beams in which the magnitude of the electric field vector is $E_s/\sqrt{2}$ and $E_p/\sqrt{2}$, respectively. The combination of the two circular polarizations yields an elliptically polarized beam: the vibration of the resultant electric field vector traces out an ellipse with semimajor and semiminor axes given by $E_M = (E_s + E_p)/\sqrt{2}$ and $E_m = |E_s - E_p|/\sqrt{2}$, respectively, and angular orientation ϕ of the semimajor axis given by Eq. (5).

It is useful for the subsequent analysis to regard the elliptical vibration as made up of two linear vibrations at right angles with amplitudes E_M and E_m, and 90° out of phase. Also, the directions of the principal axes in the first through fourth analyzer quadrants are assumed to be at 0, $\pi/4$, $\pi/2$, and $3\pi/4$ rad, respectively, with respect to the fast axis direction as shown in Fig. 6. Since the light intensity transmitted by a given quadrant is proportional to the square of the electric field amplitude resolved along the principal axis direction, it can be shown that the light intensities transmitted by the four quadrants will vary according to

$$I_1 \propto E_M^2 \cos^2\phi + E_m^2 \sin^2\phi \tag{6}$$

$$I_2 \propto E_M^2 \cos^2(\phi - \pi/4) + E_m^2 \sin^2(\phi - \pi/4) \tag{7}$$

$$I_3 \propto E_M^2 \sin^2\phi + E_m^2 \cos^2\phi \tag{8}$$

$$I_4 \propto E_M^2 \sin^2(\phi - \pi/4) + E_m^2 \cos^2(\phi - \pi/4) \tag{9}$$

The response of silicon photodiodes to light input is linear over many decades of light intensity. Therefore, to a good approximation, the four electrical current signals generated by the four element detector will have the same functional dependence on ϕ as expressed by Eqs. (6)–(9). By differentially amplifying the current signals derived from diagonally opposite quadrants, one obtains two voltage signals, $v_A \propto I_1 - I_3$ and $v_B \propto I_2 - I_4$ which, with the aid of Eqs. (5)–(9), may be expressed as

$$v_A = V \cos\delta \quad \text{and} \quad v_B = V \sin\delta \tag{10}$$

where the signal amplitude $V \propto E_M^2 - E_m^2$. It follows that the signal amplitude is a maximum when the interferometer is adjusted to make the reference and "specimen" beams equal in intensity (i.e., $E_M \to \sqrt{2}\, E_s$ or $\sqrt{2}\, E_p$ and $E_m \to 0$). One cycle of either signal corresponds to a shift of one fringe or a specimen expansion of $\lambda/2$.

Only one of the two voltage signals is actually recorded and stored (by a digital oscilloscope) during the pulse experiment. In nearly all cases, the recorded sinusoidal waveform provides sufficient information so that directional changes (if any) in the fringe shift can be determined unambiguously.

2.5. Data Acquisition and Analysis

During each pulse-heating experiment, the analog signals from the pyrometer and the interferometric system are recorded by means of two digital storage oscilloscopes, each capable of storing approximately 4000 data points with a full scale signal resolution of about 1 part in 4000. The temperature signal is recorded about every 420 μs; the time base is derived from the pyrometer chopper (see Section 2.1). For a typical heating period of 800 ms duration, the interferometer signal (v_A or v_B) is recorded every 200 μs; this allows a maximum cumulative shift of 500 fringes to be recorded with a minimum average resolution of about 8 data points per cycle of v_A or v_B (i.e., per fringe). After the pulse experiment, the recorded data is transferred from the storage oscilloscopes to a minicomputer for subsequent analyses.

In determining the specimen temperatures from the recorded radiances, corrections are made to account for the departure of the specimen from true blackbody conditions and for the light scattering effect of the optics in the pyrometer. Based on geometrical considerations only, the blackbody quality of the specimen sighting hole is estimated to be 0.98 by DeVos's method [13]. The 2% correction in radiance corresponds to an upward correction in temperature of 3.7 K at 2000 K, increasing to 8.2 K at 3000 K. For our pyrometer/specimen configuration, 1.2% of the measured radiance comes from the specimen surface surrounding the blackbody radiation hole. The correction for the scattered light depends on the emittance of the specimen surface at 0.65 μm, the effective wavelength of the pyrometer. For a value of normal spectral emittance (at 0.65 μm) of 0.4 (typical of many refractory metals at high temperatures [14]), the correction to measured radiance for scattered light yields an upward correction in temperature of 1.3 K at 2000 K, increasing to 2.9 K at 3000 K. Details of the method for computing specimen temperature from the measured spectral radiance are given in an earlier publication [6].

The linear thermal expansion of each specimen is determined from the recorded interferometric data by the following procedure. The phase δ of the interferometer signal is computed for each recorded value of v_A (or v_B) by means of Eq. (10); the interferometric signal amplitude V is redetermined for each half-cycle of the signal to account for any amplitude changes that may occur during heating of the specimen. The cumulative fringe shift corresponding to each data point is then determined from the

relation $\Delta n = \Delta\delta/2\pi$, where the phase change $\Delta\delta = \delta - \delta_0$ is measured in radians and δ_0 is the initial phase of the interferometer signal at the start of the pulse experiment.

To account for any difference between the initial temperature of the specimen and 20°C (the reference temperature), a "zero" correction is applied to the fringe count on the basis of expansion data near room temperature reported in the literature [15]. Values of $(l - l_0)/l_0$ are determined as a function of time from the corrected Δn by means of Eq. (4) and are then interpolated (in time) to yield a value of linear thermal expansion for each measured temperature of the specimen.

The final results for linear thermal expansion of a given material are expressed as a polynomial function of temperature, obtained by smoothing the combined expansion/temperature data pairs for all specimens by means of the least-squares method.

3. MEASUREMENTS

Four specimens were fabricated into precision-machined tubes from a (99.95% pure) rod of tantalum by an electro-erosion technique. Analyses by the manufacturer of the tantalum rod yielded the following impurities (in ppm by mass): O, 65; N, 30; Cr, Mo, Nb, Pb, Sn, < 30 each; Fe, 25; C, 20; Si, 15; Ca, Zr, 10 each; Ag, Al, Cu, Mg, Ni, Ti, < 10 each; H, 9; all other detected impurities, < 1 each. Nominal dimensions of the specimen tubes have been given above (Section 2.2). The width of each optical flat is approximately 3 mm, which is considerably greater than the diameter of the focused laser beam (~0.2 mm). The distance between parallel optical flats on each specimen (i.e., the specimen "length") was measured at 20.0°C by the Automated Production Technology Division at NBS using a comparative gauge block technique. The results are given in Table I along with estimates of axial nonparallelism and departure from flatness of the two reflecting surfaces.

The signal resolution of the high-speed pyrometer was optimized by dividing the temperature interval of the measurements (1500–3200 K) into six overlapping temperature ranges. This involved the use of calibrated neutral density filters in the reference lamp channel or in the unknown (specimen) channel of the pyrometer to achieve the desired range. For a given specimen, single pulse experiments were performed successively through each temperature range beginning with the lowest range.

Prior to each experiment, we adjusted a resistance in series with the specimen and the voltage from a battery bank in order to achieve the desired heating rate for a given temperature range. The specimen was then rapidly heated in a vacuum environment of about 1 mPa (~10^{-5} torr) from "room" temperature (~18°C) to the desired temperature by the

Table I. Results of Measurements Performed on the Specimen Optical Flats by a Comparative Gauge Block Technique

	Specimen number[a]			
	1	2	3	4
Distance between flats[b] (mm)	6.109	6.107	6.100	6.111
Axial parallelism[c] (min. of arc)	0.3	0.1	0.5	0.7
Flatness[d] (waves per 25 mm)	0.5	1	2	1

[a] Also the chronological order in which the specimens, in turn, were pulse heated through the temperature range between 1500 and 3200 K.

[b] Average of measurements performed at three locations along the middle two-thirds of the specimen tube at 20.0°C, yielding the specimen reference "length" l_0.

[c] Determined from the spread in measurements of specimen "length" taken at three locations along the middle two-thirds (~50 mm) of the specimen tube.

[d] Determined from measurements performed along the middle two-thirds of the specimen tube; flatness is given in terms of a wavelength of 632.8 nm.

passage of an electrical current pulse through it. The duration of the current pulse, which varied from about 750 to 800 ms, determined the maximum specimen temperature achieved in a given experiment. Heating rates varied typically from about 2500 $K \cdot s^{-1}$ for the lowest temperature range to about 4000 $K \cdot s^{-1}$ for the highest range. The elapsed time between successive pulse experiments was always greater than 20 min, thereby ensuring the equilibration of the specimen at "room" temperature.

Figure 7 is a photograph of the two traces of a dual-beam oscilloscope taken during a typical pulse experiment. The upper trace shows the time variation of the radiance from the specimen, as seen by the pyrometer, as the specimen is heated through a given temperature range. The dots forming long horizontal lines in the pyrometer output correspond to the radiance from the reference lamp when viewed directly (uppermost horizontal line) and through different calibrated attenuators. The lower trace shows the fringe shift produced by the heating of the specimen. Each cycle of the interferometer signal indicates a shift of one fringe, that is, a specimen expansion of one-half wavelength.

Upon completion of the experiments, we calibrated the high-speed pyrometer using a tungsten-filament standard lamp which, in turn, had been calibrated against the NBS Photoelectric Pyrometer by the Radiometric Physics Division at NBS. All temperatures reported in this work are based on the International Practical Temperature Scale of 1968 [16].

4. RESULTS

The linear thermal expansion of the specimen was determined at each recorded temperature from the cumulative fringe shift which, for the range

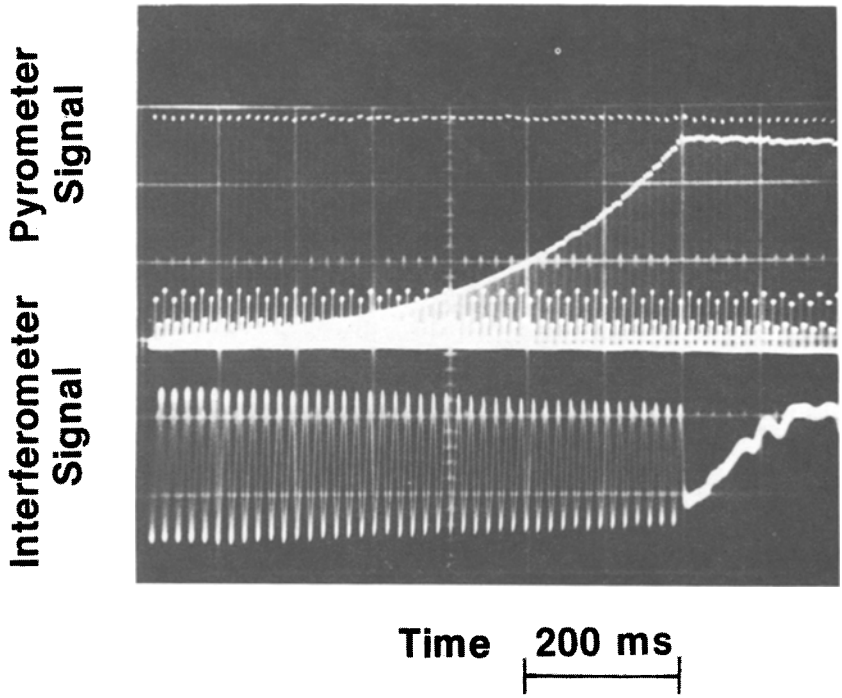

Fig. 7. Oscilloscope trace photograph of the specimen radiance, as seen by the pyrometer, and the specimen expansion, as measured by the interferometer, during a typical pulse heating experiment. Dots forming the horizontal lines in the pyrometer output correspond to the radiances from a reference source. Each cycle of interferometer output corresponds to an expansion of $\lambda/2$.

1500–3200 K, varied from about 165 to 480 fringes. The expansion/temperature data pairs for each specimen were fitted by a polynomial function of temperature by means of the least-squares method. The polynomial functions representing the results for individual specimens are given in Table II. The deviation of individual data points from the smooth function for each specimen is illustrated in Fig. 8. For some specimens, differences between data from overlapping temperature ranges can be seen as sudden breaks in the trend of data points. A measure of imprecision in our technique is given by the maximum deviation of results in the overlapping ranges from the smooth function, that is, about 0.1% at 2000 K and 0.2% at 3000 K. The random fluctuation (standard deviation $< 0.05\%$) among data points within a given temperature range is due primarily to the uncertainty in determining the phase (δ) of the interferometer signal (hence, fringe count) from a limited number of data points per fringe (about 11 at 1500 K decreasing to about 6 at 3200 K).

Table II. Results of Fitting, by Means of the Least-Squares Method, the Expansion/Temperature Data Pairs for the Individual Specimens and the Combined Data for All Four Specimens by Polynomial Functions in Temperature (in K) of the Form

$$(l - l_0)/l_0 = a_0 + a_1 T + a_2 T^2 + a_3 T^3 + a_4 T^4$$

Specimen	Number of data pairs[a]	Standard deviation[b] (%)	Polynomial coefficients[c]				
			$a_0 \times 10^4$	$a_1 \times 10^6$	$a_2 \times 10^9$	$a_3 \times 10^{12}$	$a_4 \times 10^{16}$
1	122	0.07	− 10.18	4.310	2.140	− 0.6775	1.176
2	135	0.05	16.65	−0.6042	5.511	− 1.693	2.300
3	128	0.08	6.962	1.186	4.316	− 1.357	1.959
4	131	0.05	− 14.11	4.937	1.832	− 0.6399	1.193
All specimens	516	0.20	5.141	1.445	4.160	− 1.309	1.901

[a] The number of data pairs fitted by the polynomial function represent only one out of every six expansion/temperature data points recorded in the pulse experiments.
[b] Standard deviation of an individual value of $(l - l_0)/l_0$ from the smooth function.
[c] Based on the specimen reference lengths (l_0) at 20°C.

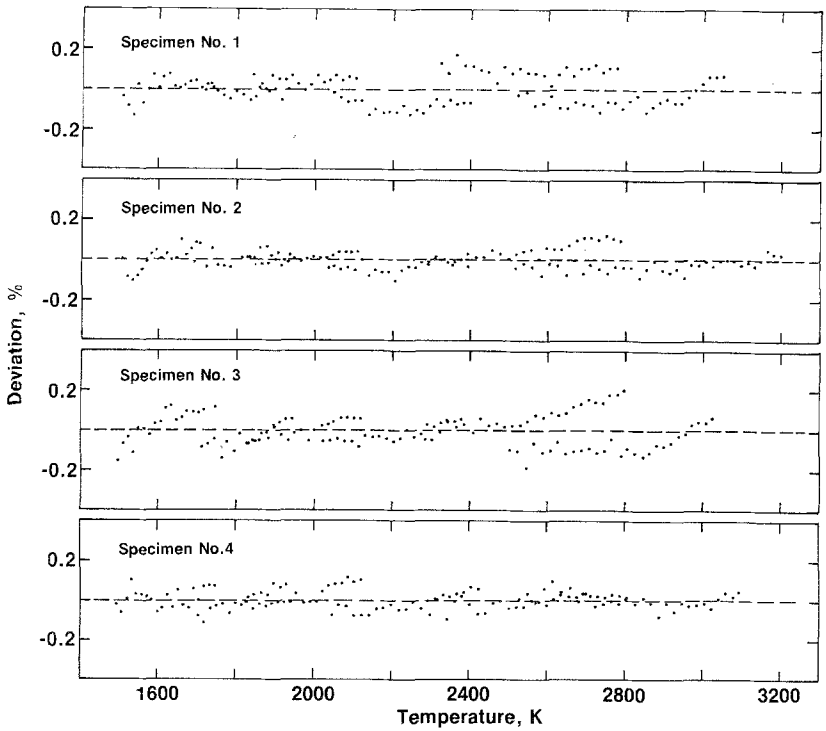

Fig. 8. Deviation of expansion/temperature data pairs from smooth functions (see Table II) representing the least-squares fits to data for the individual specimens.

Table III. Smoothed Results[a] for Linear Thermal Expansion of Tantalum

Temperature (K)	$10^2 \times (l - l_0)/l_0$ (%)	Temperature (K)	$10^2 \times (l - l_0)/l_0$ (%)
1500	0.859	2400	1.616
1600	0.936	2500	1.710
1700	1.015	2600	1.807
1800	1.096	2700	1.908
1900	1.178	2800	2.012
2000	1.261	2900	2.121
2100	1.347	3000	2.234
2200	1.434	3100	2.353
2300	1.524	3200	2.478

[a] Based on the specimen reference lengths (l_0) at 20°C.

For the final results, the expansion/temperature data pairs for the four specimens were combined and then fitted by a quartic polynomial in temperature. The function that represents the results for linear thermal expansion of tantalum (standard deviation = 0.2%) in the temperature range 1500 to 3200 K is

$$(l - l_0)/l_0 = 5.141 \times 10^{-4} + 1.445 \times 10^{-6}T + 4.160 \times 10^{-9}T^2 - 1.309 \times 10^{-12}T^3 + 1.901 \times 10^{-16}T^4 \quad (11)$$

where T is in K and l_0 is the specimen length at 20°C. Within this temperature range, the function has no inflection points. The smoothed results, as defined by Eq. (11), are given (in percent) at intervals of 100 K in Table III.

The deviation of the smoothed results for individual specimens from those of Eq. (11) is given in Fig. 9. The trend with changing temperature in the results for specimen 1 is somewhat different than that for the other three specimens. However, in all cases, the maximum deviation from the overall least-squares fit is less than 0.3% at temperatures below 2000 K and less than 0.4% at higher temperatures.

5. ESTIMATE OF ERRORS

The uncertainty in the reported values of linear thermal expansion arise from errors (random and systematic) in the measured quantities: the specimen temperature, the fringe shift, and the reference dimension of the specimen at 20°C.

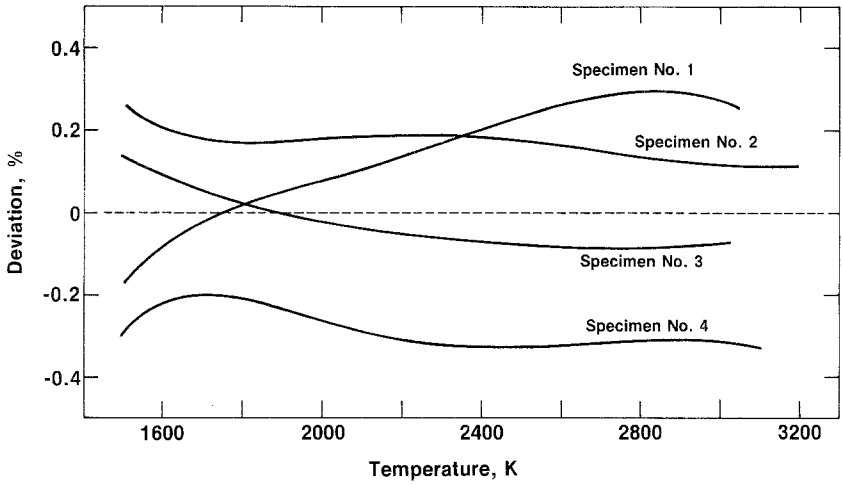

Fig. 9. Deviation of the smoothed thermal expansion results for the individual specimens from Eq. (11), which represents the least-squares fit to the combined data for the four specimens.

5.1. Errors in Temperature Measurement

A detailed analysis of the sources and magnitudes of errors involved in measuring specimen temperature with the NBS pulse heating system has been given in an earlier publication [6]. Specific items in the analysis were recomputed whenever the present conditions differed from those in the earlier publication. Table IV presents a summary of the error contributions to the measurement of temperature in the present work arising from uncertainties in: (1) pyrometry, and (2) the physical condition (geometry, material properties, etc) of the specimen.

The error in temperature measurement due to pyrometry arises from uncertainties in the standard lamp calibration and from uncertainties in the calibration and operation of the high-speed pyrometer. The maximum uncertainty in calibration of the tungsten-filament standard lamp by the Radiometric Physics Division at NBS is reported to vary from 2 K at 1400°C to 3 K at 2200°C. Therefore, we estimate the maximum error in our temperature measurements arising from the uncertainty in lamp calibration to be about 2.5 K at 2000 K and, by extrapolation, about 4 K at 3000 K. A comparison of lamp calibrations repeated during the course of several years indicates that the drift of the standard lamp between calibrations is about 1 K at 2000 K and about 2 K at 3000 K.

The uncertainties in visual alignment of the pyrometer with the standard lamp during calibration and with the blackbody radiation hole in each specimen during the pulse experiments may introduce a further error in

Table IV. Sources and Magnitudes of Errors in the Measurement of Temperature

Source	Error (K)	
	At 2000 K	At 3000 K
Pyrometry		
Standard lamp calibration	2.5	4
Drift in std. lamp calibration	1	2
Radiation source alignment	1	2
Pyrometer calibration stability	1	2
Neutral density filter calibration	1	3
Window attenuation	0.5	1
Scattered light correction	0.5	1
Specimen		
Heat transfer to clamps	1	2
Radiative heat loss	1	2
Cross-sectional nonuniformity	3	6
Blackbody quality	1	2
Total error in temperature[a]	5	10

[a] Square root of the sum of squares of the individual errors.

temperature measurement. Based on the analysis of experimental results from a series of tests with steady-state radiation sources, the error arising from this uncertainty is estimated to be about 1 K at 2000 K and about 2 K at 3000 K. The uncertainty in stability of the pyrometer calibration was determined by two successive calibrations (within 1 day) and found to be not more than 1 and 2 K at temperatures of 2000 and 3000 K, respectively.

Further errors in temperature arise from uncertainties in calibrating the neutral density filters used in establishing the different temperature ranges of the pyrometer. Based on repeated measurements of filter attenuation conducted with the pyrometer and a steady-state radiation source, it is estimated that the uncertainty in filter calibration contributes an error in temperature of about 1 K at 2000 K and about 3 K at 3000 K.

Similar tests on the attenuation of the specimen chamber window yield an estimated uncertainty in temperature of about 0.5 K at 2000 K and 1 K at 3000 K. The specimen chamber window was also checked for changes in attenuation due to vapor deposition before and after each series of pulse experiments on a given specimen, but no changes were detected.

The uncertainty in the correction for light scattered by the pyrometer optics is approximately 0.1% in radiance. This corresponds to an error in temperature of 0.5 K at 2000 K and 1 K at 3000 K.

The errors in temperature measurement due to the specimen conditions are primarily the result of temperature nonuniformities within the

specimen which arise from (1) heat transfer to the end clamps, (2) radiative heat loss from the specimen surface, and (3) small variations in cross-sectional area along the length of the specimen. The magnitude of the axial temperature gradient arising from (1) can be estimated by solving the transient heat conduction equation [17], based on the assumption of constant properties; computations indicate that the average temperature in the central portion of the tube (excluding about 12 mm of length nearest each end-clamp) is approximately 1 K lower than the midpoint value at 2000 K, and about 2 K lower at 3000 K. The maximum radial temperature difference across the thin specimen wall arising from (2) is estimated, by a similar analysis (see [6]), to be about 1 K at 2000 K and 2 K at 3000 K. The measured temperatures were not corrected for these small axial and radial temperature gradients. Item (3), which can be estimated from potentiometric measurements of resistance (at room temperature) across small intervals along the tube length, may create temperature nonuniformities as large as 3 K at 2000 K and 6 K at 3000 K.

The uncertainty in the correction for the departure of the specimen sighting hole from true blackbody conditions is about 0.5% in radiance. This contributes an error in temperature of approximately 1 K at 2000 K and 2 K at 3000 K.

Assuming that the various error contributions are uncorrelated, we conclude that the total (random and systematic) error in the measurement of temperature is not greater than 5 K at 2000 K and 10 K at 3000 K. These errors contribute uncertainties in the reported values for linear thermal expansion of about 0.3% at 2000 K and 0.5% at 3000 K.

To evaluate our estimates of specimen temperature nonuniformities and their effects on expansion results, a series of pulse experiments were performed in a single temperature range on specimen 2 under various operating conditions. The smoothed results are presented in Fig. 10 as a deviation plot in which results from experiment 4, performed under "normal" operating conditions (heating rate $\sim$3200 $K \cdot s^{-1}$), serve as the "zero" line (or baseline). Experiments 1–3 were conducted at a considerably higher heating rate ($\sim$7000 $K \cdot s^{-1}$), whereas experiments 5–7 were performed under normal heating rates but with the interferometer raised sufficiently ($\sim$6 mm) so as to exclude the pyrometric sighting hole from the "effective" specimen involved in interferometry (about 1 mm of the tube length).

As may be seen in Fig. 10, the effect of approximately doubling the heating rate on the expansion results is about 0.2% or less. An increase in heating rate will tend to enhance any variations in temperature due to nonuniformities in cross-sectional area along the specimen tube but, at the same time, it will reduce the magnitude of (small) axial and radial temperature gradients in the specimen. Also, it may be seen that the linear

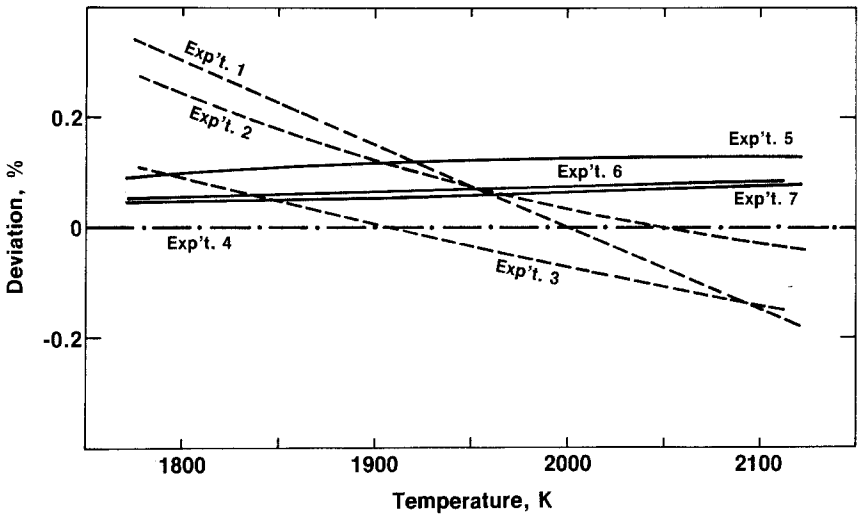

Fig. 10. Deviation of smoothed thermal expansion results for experiments conducted under various operating conditions from those of experiment 4, which was performed under normal conditions (heating rate ~3200 $K \cdot s^{-1}$). Experiments 1–3 were conducted at a higher heating rate (~7000 $K \cdot s^{-1}$), whereas in experiments 5–7, the pyrometric sighting hole was excluded from the "effective" specimen involved in the interferometry (~1 mm of the specimen tube length).

expansion of an "effective" specimen above the sighting hole is about the same, within our measurement precision,[2] as the expansion of an "effective" specimen which includes the sighting hole. Therefore, the results of experiments 4–7 suggest that axial variations of temperature in the vicinity of the blackbody radiation hole (due to nonuniformities in cross-sectional area) are rather small.

In summary, the estimates of error in the measurement of temperature arising from specimen temperature nonuniformities given above appear to be consistent with the results of the seven test experiments. In addition, the results of experiment 4 were compared with those obtained in an earlier experiment on specimen 2 under similar operating conditions. It was found that the results of experiment 4 are about 0.2% lower than the earlier expansion values. This "decrease" in the measured expansion appears to be consistent with an observed decrease (0.1–0.2%) in l_0 as a result of repeated pulse heating (see Section 5.3).

[2]The reproducibility of results obtained by experiments 5–7 indicates that the imprecision of our expansion measurements is of the order of 0.1% at temperatures around 2000 K. This agrees with the estimates of imprecision given earlier in Section 4.

5.2. Errors in Fringe Count

The estimated errors in the determination of cumulative fringe count are summarized in Table V; the error contributions arise from uncertainties in: (1) interferometry, and (2) the specimen conditions.

The background drift in the interferometric signal during pulse heating was estimated from the (small) random fluctuation in the signal prior to each experiment, yielding a maximum uncertainty of 0.2 fringe. The limitation in number of data points recorded per fringe (about 10 at 2000 K and 6 at 3000 K) contributes a further random uncertainty in the fringe count of about 0.1 fringe at 2000 K and less than 0.2 fringe at 3000 K. The fringe resolution of the present work corresponds to a measurement sensitivity of about 5 $\mu m \cdot m^{-1}$ at 2000 K and 9 $\mu m \cdot m^{-1}$ at 3000 K.

The error in determining the "room" temperature of the "effective" specimen prior to each pulse experiment is estimated to be not greater than 1 K. This error contributes an uncertainty in the "zero" correction applied to the cumulative fringe count of 0.15 fringe.

The deviation of either "front" surface or "back" surface reflection (or both) from the assumed condition of normal incidence (Section 2.3) will contribute some error to the fringe count. The maximum deviation occurs in the case of the "front" surface reflection as a result of the alignment procedure to prevent the parasitic "ghost" of the "front" surface reflection transmitted by PB1 (see Fig. 5) from reentering the laser cavity and thus reducing the laser coherence: the laser is aligned approximately 1.5 mm off the optic axis of lens L1 (focal length ~100 mm). However, one can show that even for this case of maximum deviation ($\sim 1.5 \times 10^{-2}$ rad) from

Table V. Sources and Magnitudes of Errors in the Measurement of Fringe Shift

	Error, number of fringes	
Source	At 2000 K	At 3000 K
Interferometry		
Background signal drift	0.2	0.2
Fringe resolution	0.1	0.2
"Zero" correction	0.15	0.15
Specimen		
Axial nonparallelism of flats	0.35	0.7
Rotational stability	0.3	0.6
Departure from flatness	0.05	0.1
Total error in fringe count[a]	0.6	1

[a] Square root of the sum of squares of the individual errors.

normal incidence, the resulting error in fringe count is negligible when compared with errors from other sources.

The absorption by the entrance/exit chamber windows of thermal radiation from the specimen during pulse heating will tend to change the optical path length of the "specimen" beam because of the nonzero temperature coefficients for expansivity and refractive index of the glass. To determine the magnitude of this effect, a series of pulse experiments were performed with the interferometer realigned so that the "specimen" beam passed directly through the experiment chamber via the entrance/exit windows, without undergoing reflections by the specimen. The results indicate that any shift in fringe pattern due to heat absorption by the window during a pulse experiment is considerably smaller than the random background fluctuation of the fringes.

The major sources of error in the fringe shift measurements arise from uncertainties associated with movement of the specimen during pulse heating. As a result of axial expansion of the specimen, the center portion of the tubular specimen moves downward (through the plane of the interferometer) approximately 0.5 mm at 2000 K and 1 mm at 3000 K. Therefore, the departure by the pair of optical flats from exact axial parallelism will contribute an uncertainty in measuring the change in specimen "length," that is, in determining the cumulative fringe count. On the basis of data given in Table I, the uncertainty in fringe count arising from axial nonparallelism of the flats is estimated to be not larger than 0.35 fringe at 2000 K and 0.7 fringe at 3000 K.

The rotational movement by the specimen during the experiment will also contribute an uncertainty in measuring the specimen "length." In the Appendix, we derive an expression (Eq. A7) which gives the apparent fractional length change $\delta l/l$ as a function of specimen rotation $\delta\theta$ and misalignment d between successive reflections of the "specimen" beam. On the basis of several realignments of the interferometer with a given specimen, it is estimated that the ratio d/l is not greater than 0.07. The rotational movement was determined by reflecting an auxiliary laser beam from a third optical flat (directly opposite from the pyrometric sighting hole) on the specimen and measuring the displacement of the reflected beam. The results yield an estimated upper limit to $\delta\theta$ of 2×10^{-4} rad at 2000 K and 4×10^{-4} rad at 3000 K. Based on these estimates, Eq. (A7) yields a maximum uncertainty in fractional length change (due to specimen rotation) of about 1.5×10^{-5} at 2000 K and 3×10^{-5} at 3000 K; the corresponding uncertainties in fringe count are 0.3 and 0.6 fringe at the respective temperatures.

Taking into account the specimen movement during pulse heating, we estimate that the departure from flatness (see Table I) by the pair of

reflecting surfaces contributes an additional combined uncertainty in fringe count of about 0.05 fringe at 2000 K and 0.1 fringe at 3000 K.

It may be concluded that, if no correlations exist among the various error contributions, the total (random and systematic) error in the measurement of fringe count is about 0.6 fringe at 2000 K and 1 fringe at 3000 K. These errors correspond to an uncertainty in linear thermal expansion of about 0.3% at both temperatures.

5.3. Errors in Specimen "Length" at 20°C

The values of linear thermal expansion reported in this work are based on the specimen "lengths" (l_0) measured at 20.0°C prior to any pulse heating experiments. The maximum uncertainty in these measurements is estimated to be about 0.003 mm or 0.05%. Upon completion of all pulse experiments, the "lengths" of the specimens were remeasured at 20.0°C, yielding values for specimens 1, 3, and 4 that were about 0.1% smaller than those obtained prior to the pulse experiments; the decrease in "length" of specimen 2, which was subjected to seven additional pulse experiments (Section 5.1), was about 0.2%. A possible explanation of this effect is that, with each successive pulse heating, there is a partial annealing of stresses in the specimen tube (induced during fabrication) thereby creating a (small) permanent change in the specimen dimensions; since each specimen was successively heated through six temperature ranges beginning with the lowest range, the cumulative change in l_0 would be greatest for the highest range. However, no corrections to the expansion results for these (small) systematic changes in l_0 were attempted in the present work. Thus, it is estimated that the total uncertainty (systematic and random) in the value of l_0 contributes an error in $(l - l_0)/l_0$ of not greater than 0.2% at 2000 K and 0.3% at 3000 K.

5.4. Summary of Error Estimates

The estimates of uncertainty in our determination of thermal expansion arising from measurements of specimen temperature, fringe count, and specimen "length" l_0 are summarized in Table VI. It may be concluded that the maximum possible error (random plus systematic) in our reported values for linear thermal expansion of tantalum is about 1% at 2000 K and not greater than 2% at 3000 K.

6. DISCUSSION

A comparison of the present results for tantalum as expressed by Eq. (11) with expansion data found in the literature is given in Fig. 11. The only expansion measurements on tantalum at temperatures approaching the

Table VI. Estimated Error Contributions of the Measured Quantities to the Reported Values of Linear Thermal Expansion

Measured quantity	Error (%)	
	At 2000 K	At 3000 K
Temperature	0.3	0.5
Fringe count	0.3	0.3
Length at 20°C	0.2	0.3
Maximum total error	1	<2

melting point (~3270 K) appear to be those of Rasor and McClelland [18]. All other expansion data reported for tantalum were obtained at temperatures less than about 2700 K. The values of expansion reported by Rasor and McClelland [18], Worthing [19], and Conway and Losekamp [20] were obtained by the twin-telemicroscope method. Edwards et al. [21] and Waseda et al. [22] obtained their expansion data using x-ray diffraction techniques. The expansion values reported by Amonenko et al. [23] were determined by push-rod dilatometry. The data disagree by as much as 10% through the temperature ranges common to the different investigations.

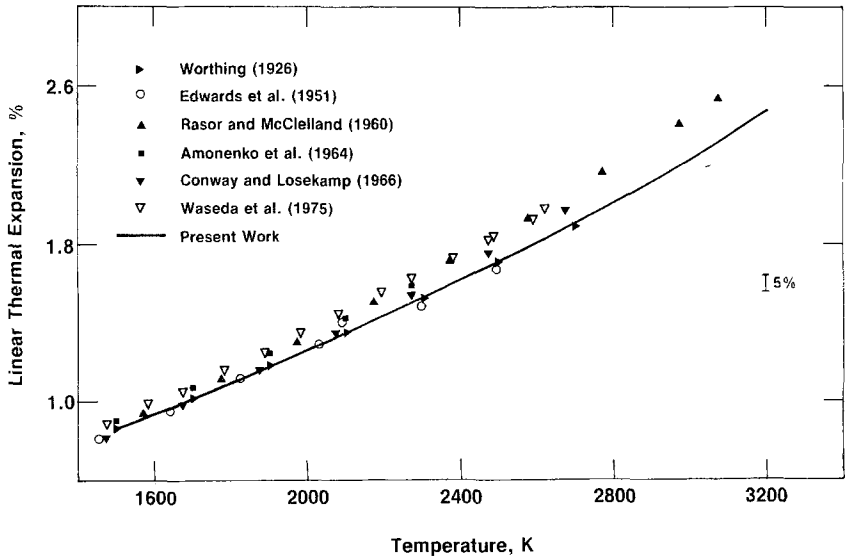

Fig. 11. Linear thermal expansion of tantalum: present work and data reported in the literature.

However, the reported data do not show any significant bias towards a given steady-state measurement technique.

The expansion values determined by Worthing and by Edwards et al. are in rather good agreement with results of the present work. The expansion data reported by Conway and Losekamp agree with those of the present work within the combined experimental errors of the two investigations. However, the expansion results reported by the remaining investigators, including Rasor and McClelland, whose data extend well beyond 2700 K, are considerably higher than our results.

In summary, the results of the present study show that our transient interferometric technique is capable of measuring the linear thermal expansion of metals between room temperature and temperatures in the range 1500 K to their melting points with an estimated error of less than 2%; the measurement imprecision is estimated to be about 0.2%. The present measurements on tantalum also indicate that the interferometric measurement system, in its present configuration, is capable of measuring thermal expansion of a 6 mm specimen with a sensitivity of better than 10 $\mu m \cdot m^{-1}$.

ACKNOWLEDGMENTS

This work was supported in part by the U.S. Air Force Office of Scientific Research. The help extended by M. S. Morse with the electronic instrumentation is greatly appreciated. The authors also express their gratitude to R. J. Hocken for the helpful discussions concerning interferometry and to C. D. Tucker for the accurate measurements of specimen "lengths" at 20°C.

APPENDIX

In this section, we derive the functional dependence of the apparent change in specimen "length" (δl) arising from rotational movement, on specimen rotation ($\delta\theta$) and on the departure (d) from colinear alignment of the successive reflections from opposite sides of the specimen. The quantities $\delta\theta$ and d as well as other quantities used in the following analysis are defined in Fig. 12; quantities with a subscript 1 refer to the "front" surface reflection, whereas those with a subscript 2 refer to the "back" surface reflection.

In our analysis, the rotation $\delta\theta$ and the respective displacements y_1 and y_2 of the component beam from the laser and the "back" surface reflection are assumed sufficiently small so that the reflection points continue to

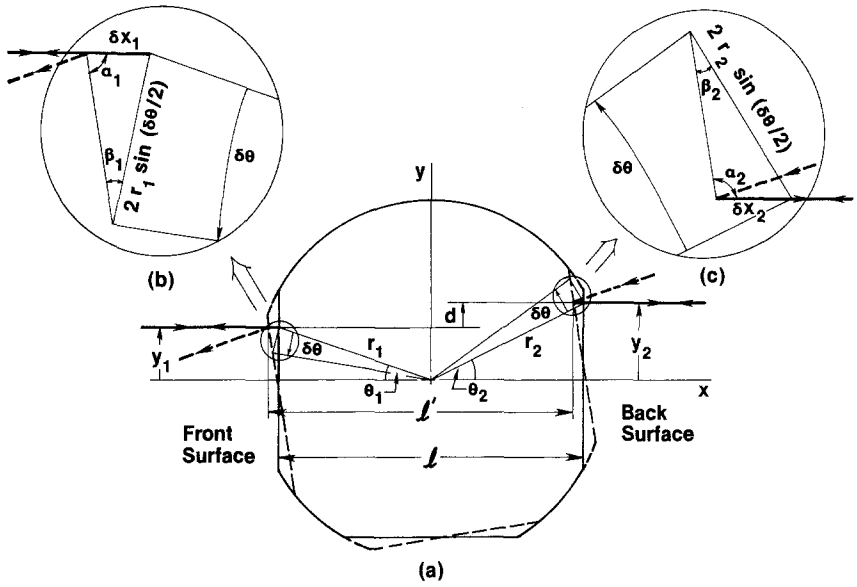

Fig. 12. Diagrams illustrating the effect of rotational movement of the specimen on the successive "front" surface/"back" surface reflections: (a) the apparent change in length $\delta l = l' - l$ depends not only on the amount of rotation $\delta\theta$ but also on the departure d from colinear alignment of the successive reflections; (b) and (c) give expanded views of the respective regions around the "front" surface and the "back" surface reflection points.

remain in the focal planes of lenses L1 and L2 of the interferometer; in other words, the changes in positions of the "front" and "back" surface reflection points are much smaller than the focal lengths of L1 and L2. In this approximation, a specimen rotation will only yield a (small) lateral displacement of the "front" surface reflection as it leaves lens L1. By tracing the path of this beam through optical components PB1, PP2, M2, and PB2 (see Fig. 5), one can show that the lateral displacement of the "specimen" beam is exactly compensated by lens L2, yielding a negligible lateral displacement of the "back" surface reflection. This means that the "specimen" beam remains superimposed with the reference beam as they enter the detector irrespective of small rotational movements by the specimen. Therefore, the change in optical path length of the "specimen" beam, in this approximation, arises entirely from the apparent change in specimen "length."

The apparent change in length $\delta l = l' - l$ may be expressed as

$$\delta l = \delta x_2 - \delta x_1 \tag{A1}$$

where $\delta x_1 = x_1' - x_1$ and $\delta x_2 = x_2' - x_2$ are the changes in position of the "front" and "back" surface reflection points, respectively; the primed quantities refer to conditions after rotation of the specimen. By applying the law of sines to Fig. 12(b) and (c), one obtains

$$\delta x_1 = -\left[2r_1 \sin(\delta\theta/2)\right] \sin \beta_1 / \sin \alpha_1 \tag{A2}$$

and

$$\delta x_2 = -\left[2r_2 \sin(\delta\theta/2)\right] \sin \beta_2 / \sin \alpha_2 \tag{A3}$$

where positive values of $\delta\theta$ indicate a counter clockwise rotation of the specimen. Consideration of various quantities in the diagrams of Fig. 12 yields the following relationships:

$$\alpha_1 = \frac{\pi}{2} - \delta\theta, \qquad \alpha_2 = \frac{\pi}{2} + \delta\theta$$

$$\beta_1 = \theta_1 + \frac{\delta\theta}{2}, \qquad \beta_2 = \theta_2 - \frac{\delta\theta}{2}$$

$$\sin\theta_1 = y_1/r_1, \qquad \sin\theta_2 = y_2/r_2$$

$$\cos\theta_1 = l/2r_1, \qquad \cos\theta_2 = l/2r_2$$

which allows Eqs. (A2) and (A3) to be expressed as

$$\delta x_1 = -l(\sec\delta\theta - 1)/2 - y_1 \tan\delta\theta \tag{A4}$$

and

$$\delta x_2 = l(\sec\delta\theta - 1)/2 - y_2 \tan\delta\theta \tag{A5}$$

Finally, by substituting Eqs. (A4) and (A5) into (A1), we can express the apparent fractional change in specimen "length" as

$$\delta l/l = \sec\delta\theta - 1 - (d/l)\tan\delta\theta \tag{A6}$$

where the departure from colinear alignment is given by $d = y_2 - y_1$.

In our interferometric technique, the rotational movement of the specimen is typically less than 10^{-3} rad. Therefore, to a good approximation, $\delta l/l$ is given by the lowest-order terms in the Taylor series expansions about $\delta\theta = 0$ for $\sec\delta\theta$ and $\tan\delta\theta$:

$$\delta l/l = (\delta\theta)^2/2 - (d/l)\delta\theta \tag{A7}$$

It is clear from Eq. (A7) that any departure from colinear alignment significantly increases the uncertainty in our expansion measurements arising from rotational instability of the specimen.

REFERENCES

1. A. Cezairliyan, *High Temp.-High Press.* **11**:9 (1979).
2. R. A. Finch and R. E. Taylor, *Rev. Sci. Instrum.* **40**:1195 (1969).
3. G. R. Gathers, J. W. Shaner, and R. L. Brier, *Rev. Sci. Instrum.* **47**:471 (1976).
4. A. Cezairliyan, *Rev. Sci. Instrum.* **42**:540 (1971).
5. G. Ruffino, A. Rosso, L. Coslovi, and F. Righini, in *AIP Conference Proceedings No. 17 —Thermal Expansion*, R. E. Taylor and G. L. Denman, eds. (American Institute of Physics, New York, 1974), p. 159.
6. A. Cezairliyan, M. S. Morse, H. A. Berman, and C. W. Beckett, *J. Res. Natl. Bur. Stand* (U.S.) **74A**:65 (1970).
7. A. Cezairliyan, *J. Res. Natl. Bur. Stand.* (U.S.) **75C**:7 (1971).
8. A. P. Miiller and A. Cezairliyan, in *Thermal Expansion 6*, I. D. Peggs, ed. (Plenum Press, New York, 1978), p. 131.
9. G. M. Foley, *Rev. Sci. Instrum.* **41**:827 (1970).
10. W. R. C. Rowley, *IEEE Trans. Instrumentation and Measurement* **IM-15**:146 (1966).
11. J. Dyson, *Interferometry as a Measuring Tool* (Hunt Barnard Printing Ltd., Aylesbury, 1970).
12. R. J. Hocken, National Bureau of Standards, private communication.
13. J. C. DeVos, *Physica* **20**:669 (1954).
14. Y. S. Touloukian and D. P. DeWitt, *Thermophysical Properties of Matter, Vol. 7, Thermal Radiative Properties* (IFI/Plenum, New York, 1970).
15. Y. S. Touloukian, R. K. Kirby, R. E. Taylor, and P. D. Desai, *Thermophysical Properties of Matter, Vol. 12, Thermal Expansion* (IFI/Plenum, New York, 1975).
16. The International Committee for Weights and Measures, *Metrologia* **5**:35 (1969).
17. H. S. Carslaw and J. C. Jaeger, *Conduction of Heat in Solids* (Oxford University Press, Oxford, 1959).
18. N. S. Rasor and J. D. McClelland, *J. Phys. Chem. Solids* **15**:17 (1960).
19. A. G. Worthing, *Phys. Rev.* **28**:190 (1926).
20. J. B. Conway and A. C. Losekamp, *Trans. Met. Soc. AIME* **236**:702 (1966).
21. J. W. Edwards, R. Speiser, and H. L. Johnston, *J. Appl. Phys.* **22**:424 (1951).
22. Y. Waseda, K. Hirata, and M. Ohtani, *High Temp.-High Press.* **7**:221 (1975).
23. V. M. Amonenko, P. N. Vyugov, and V. S. Gumenyuk, *High Temp.* (USSR) **2**:22 (1964).